Estimation of Involuntary Impedance in Multi-joint Arm Movements

Hendrik Börner * **Satoshi Endo** * **Sandra Hirche** *

* *Chair of Information-oriented Control, Department of Electrical and Computer Engineering, Technical University of Munich, 80333 Munich, Germany, {hendrik.boerner, s.endo, hirche}@tum.de.*

Abstract: Stability analysis in physical human-robot interaction requires consideration of human feedback behavior. In unpredictable scenarios, where voluntary cognitive feedback is too slow to guarantee desired task execution, the central nervous system relies on intrinsic and involuntary reflexive feedback. In this work, we present a method for the estimation of the combined effects of intrinsic and involuntary reflexive feedback in multi-joint arm movements, termed involuntary impedance. We apply external force perturbations that are specifically designed to evoke feedback jerk, which can be isolated by application of a high pass filter, and limit the duration of the estimation interval to guarantee the exclusion of voluntary feedback. The isolation of the feedback behavior is validated in simulation and the estimation of the involuntary impedance components is evaluated in an experiment with human participants.

Keywords: Involuntary Impedance, Impedance Estimation, Human Motor Control, Robotics

1. INTRODUCTION

Technological advancements in the area of cyber-physical and human systems are enabling robotic assistance through physical human-robot interaction (pHRI). Possible areas of application include, but are not limited to, industrial, domestic, and medical domains. During pHRI, unstable interaction behavior must be avoided to guarantee safety and comfort of the human. Therefore, it is necessary to incorporate human behavior in the control design process.

During execution of a desired motor task, joint torques produced by the neuromuscular system are composed of a feedforward and a feedback component (Tee et al., 2004). The feedback component counteracts deviations due to unpredictable dynamics, which may be caused by external perturbations (Gomi and Kawato, 1997), incorrect internal models (Franklin and Wolpert, 2011), and neural noise (Slifkin and Newell, 1999). It consists of effects of intrinsic viscoelastic properties, involuntary reflexes, and voluntary cognitive feedback (Gomi and Osu, 1998). As voluntary cognitive feedback possesses the longest delays, it may be insufficient to guarantee desired task execution in unpredictable scenarios (Franklin and Wolpert, 2011). In such situations, the central nervous system (CNS) must rely on intrinsic and involuntary reflexive feedback.

These two feedback components can be modeled by the mechanical impedance components damping and stiffness (Dolan et al., 1993). Due to the length- and velocity-tension relationships of muscle fibers, both depend on joint angles, angular velocities, and muscle activations (Mussa-Ivaldi et al., 1985). The dependency on muscle activations enables a priori cognitive modulation by the CNS (Darainy et al., 2007). The analysis of such cognitive modulation strategies in experiments that emulate realistic pHRI may provide valuable insights for the control design process. However, it first requires an estimation method, which is compatible with the limited interval, in which only the intrinsic and involuntary reflexive feedback are active, and which is applicable to tasks that emulate pHRI.

Gomi and Kawato (1997) perform impedance estimation in multi-joint arm movements by application of external force perturbations and least squares estimation in a 280 ms interval. A similar method is used by Erden and Billard (2015) to estimate impedance in a 250 ms interval during manual welding with a robot. Burdet et al. (2000) use position perturbations with constant deviations to exclusively estimate stiffness in a 60 ms interval that starts 120 ms after perturbation onset. A similar method is used by Darainy et al. (2007) to estimate stiffness in a 50 ms interval that starts 250 ms after perturbation onset. Piovesan et al. (2013) use a time-frequency analysis that is only applicable to free, unfettered movements to estimate impedance 135 ms after perturbation onset. In summary, to the best of the author's knowledge, previous methods either exclusively estimate stiffness, do not guarantee exclusion of voluntary feedback, or are confined to free, unfettered movements that are unable to emulate pHRI.

In this work, we present a method for the estimation of the combined effects of intrinsic and involuntary reflexive feedback in multi-joint arm movements, which we term involuntary impedance. External force perturbations are applied to evoke deviations during two-dimensional point to point arm movements. These force perturbations are designed such that the jerk frequency content of the evoked feedback behavior lies outside the jerk frequency content of the unperturbed movements. Consequently, the feedback behavior can be isolated by application of

⋆ This research is partly supported by the ERC Starting Grant "Control based on Human Models (con-humo)" under the grant agreement no. 337654.

a high pass filter to the jerk of the perturbed movement. We limit the duration of the estimation interval in order to guarantee the exclusion of voluntary feedback and estimate the involuntary impedance components by least squares analysis. The isolation of the feedback behavior is validated with a simulated model of the human arm and the estimation of the involuntary impedance components is evaluated in an experiment with human participants.

The remainder of this paper is structured as follows: Section 2 contains the formulation of the involuntary impedance estimation problem. The proposed method is introduced in Section 3. The isolation of the feedback behavior is validated with simulated data in Section 4 and the estimation of the involuntary impedance components is evaluated with experimental data in Section 5.

2. PROBLEM SETTING

We model the human arm as a two-link system that is constrained to movement in the horizontal plane:

$$\boldsymbol{\tau}_{\text{int}} = M_q(\boldsymbol{q})\ddot{\boldsymbol{q}} + C(\boldsymbol{q}, \dot{\boldsymbol{q}}) - \boldsymbol{\tau}_{\text{ext}} \ , \tag{1}$$

where $\boldsymbol{q}$ is the 2 degree of freedom (DoF) arm configuration in joint space, M_q is the inertia matrix, C represents the Coriolis and centrifugal forces, $\boldsymbol{\tau}_{\text{int}}$ are internal torques and $\boldsymbol{\tau}_{\text{ext}}$ are external torques (Gomi and Kawato, 1997).

The internal torques $\boldsymbol{\tau}_{\text{int}}$ are produced by the muscle tensions $\boldsymbol{m}$, which depend on the muscle lengths $\boldsymbol{\lambda}$, the respective derivatives $\dot{\boldsymbol{\lambda}}$, and the muscle activations $\boldsymbol{a}$:

$$\boldsymbol{\tau}_{\text{int}} = J_m(\boldsymbol{\lambda})^{\mathsf{T}} \boldsymbol{m}(\boldsymbol{\lambda}, \dot{\boldsymbol{\lambda}}, \boldsymbol{a}) \ . \tag{2}$$

The muscle tensions $\boldsymbol{m}$ are transformed to joint space by the muscle Jacobian $J_m(\boldsymbol{\lambda})$, which contains the muscle length $\boldsymbol{\lambda}$ dependent muscle moment arms.

During motor task execution, the muscle activations $\boldsymbol{a}$ consist of a feedforward term $\boldsymbol{a}_{\text{FF}}$, a feedback term $\boldsymbol{a}_{\text{FB}}$, and a neural noise term $\boldsymbol{a}_{\text{N}}$ (Franklin et al., 2008):

$$\boldsymbol{a} = \boldsymbol{a}_{\text{FF}} + \boldsymbol{a}_{\text{FB}} + \boldsymbol{a}_{\text{N}} \ . \tag{3}$$

The feedback muscle activations $\boldsymbol{a}_{\text{FB}}$ consist of multiple components produced at different delays after the onset of unpredictable dynamics (Franklin and Wolpert, 2011):

$$\boldsymbol{a}_{\text{FB}} = \begin{cases} 0 & \forall\ \Delta t \in [0, \delta_{\text{r}}] \\ \boldsymbol{a}_{\text{FB,r}}(\boldsymbol{\lambda}, \dot{\boldsymbol{\lambda}}) & \forall\ \Delta t \in \,]\delta_{\text{r}}, \delta_{\text{v}}] \\ \boldsymbol{a}_{\text{FB,r}}(\boldsymbol{\lambda}, \dot{\boldsymbol{\lambda}}) + \boldsymbol{a}_{\text{FB,v}}(\boldsymbol{\theta}) & \forall\ \Delta t > \delta_{\text{v}} \end{cases} , \tag{4}$$

where $\boldsymbol{a}_{\text{FB,r}}$ and $\boldsymbol{a}_{\text{FB,v}}$ represent reflexive and voluntary feedback muscle activations, δ_{r} and δ_{v} are the associated delays, and $\Delta t = t - t_0$ is the time after the onset of the unpredictable dynamics at $t = t_0$. In the interval $]\delta_{\text{r}}, \delta_{\text{v}}]$, there are only reflexive feedback muscle activations $\boldsymbol{a}_{\text{FB,r}}$, which are affected by neural conduction delays. The fastest reflexive feedback is the short-latency stretch reflex with a delay $\delta_{\text{r,s}}$ in the order of $10 - 40$ ms (Matthews, 1991). As cognitive feedback adaptation is not yet possible in this interval, the reflexive feedback muscle activations $\boldsymbol{a}_{\text{FB,r}}$ only depend on the muscle lengths $\boldsymbol{\lambda}$ and the respective derivatives $\dot{\boldsymbol{\lambda}}$. For $\Delta t > \delta_{\text{v}}$, there are also voluntary feedback muscle activations $\boldsymbol{a}_{\text{FB,v}}$, which depend on task-specific input parameters $\boldsymbol{\theta}$ (Todorov and Jordan, 2002). Feedback of sensory information to the CNS is subject to neural conduction and receptor dynamics delays. In case of proprioceptive sensory information for motion perception, these delays are in the order of 100 ms. The conduction delay of a descending motor command to the arm muscles is approximately 15 ms (Merton and Morton, 1980). Thus, the minimum delay δ_{v} is in the order of 115 ms.

Analogous to the muscle activations $\boldsymbol{a}$, the internal torques $\boldsymbol{\tau}_{\text{int}}$ are composed of a feedforward term $\boldsymbol{\tau}_{\text{FF}}$, a feedback term $\boldsymbol{\tau}_{\text{FB}}$, and a neural noise term $\boldsymbol{\tau}_{\text{N}}$ (Tee et al., 2004):

$$\boldsymbol{\tau}_{\text{int}} = \boldsymbol{\tau}_{\text{FF}} + \boldsymbol{\tau}_{\text{FB}} + \boldsymbol{\tau}_{\text{N}} \ . \tag{5}$$

The feedback term $\boldsymbol{\tau}_{\text{FB}}$ is composed of restoring torques towards the desired behavior (Lakatos et al., 2011):

$$\boldsymbol{\tau}_{\text{FB}} = \begin{cases} \boldsymbol{\tau}_{\text{FB,i}} & \forall\ \Delta t \in [0, \delta_{\text{r}}] \\ \boldsymbol{\tau}_{\text{FB,i}} + \boldsymbol{\tau}_{\text{FB,r}} & \forall\ \Delta t \in \,]\delta_{\text{r}}, \delta_{\text{v}}] \\ \boldsymbol{\tau}_{\text{FB,i}} + \boldsymbol{\tau}_{\text{FB,r}} + \boldsymbol{\tau}_{\text{FB,v}} & \forall\ \Delta t > \delta_{\text{v}} \end{cases} , \tag{6}$$

where $\boldsymbol{\tau}_{\text{FB,i}}$, $\boldsymbol{\tau}_{\text{FB,r}}$, and $\boldsymbol{\tau}_{\text{FB,v}}$ are intrinsic, reflexive, and voluntary feedback torques, respectively (Tee et al., 2004).

In this work, in order to guarantee the exclusion of voluntary feedback torques $\boldsymbol{\tau}_{\text{FB,v}}$, we limit the duration of the impedance estimation interval T_{est}. According to (4), the voluntary feedback muscle activations $\boldsymbol{a}_{\text{FB,v}}$ depend on the task-specific input parameters $\boldsymbol{\theta}$. Because of the goal-directed nature of the point to point movements, it is assumed that these parameters are predominantly determined by the joint angles $\boldsymbol{q}$. Due to the design of the perturbation, the onset of the perturbation is followed by an interval of duration T_{dev}, in which the evoked feedback behavior does not yet possess noticeable deviations. Thus, in this work, the delay of the voluntary feedback muscle activations $\boldsymbol{a}_{\text{FB,v}}$ is assumed $\delta_{\text{v,dev}} = \delta_{\text{v}} + T_{\text{dev}}$ and the duration of the estimation interval $T_{\text{est}} = \delta_{\text{v,dev}}$. Due to the various delays δ_{r} of the reflexive feedback torques $\boldsymbol{\tau}_{\text{FB,r}}$ and the short duration of the interval, in which only the intrinsic feedback torques $\boldsymbol{\tau}_{\text{FB,i}}$ are active, differentiation of the respective contributions is difficult (Tee et al., 2004). Therefore, we summarize the effects of both terms in the involuntary feedback term

$$\overline{\boldsymbol{\tau}}_{\text{FB}} = \begin{cases} \boldsymbol{\tau}_{\text{FB,i}} & \forall\ \Delta t \in [0, \delta_{\text{r}}] \\ \boldsymbol{\tau}_{\text{FB,i}} + \boldsymbol{\tau}_{\text{FB,r}} & \forall\ \Delta t \in \,]\delta_{\text{r}}, T_{\text{est}}] \end{cases} . \tag{7}$$

This approach is common to impedance estimation studies and similarly applied to significantly longer estimation intervals than the one in this work (Gomi and Kawato, 1997; Burdet et al., 2000; Erden and Billard, 2015).

For small deviations, the feedback behavior evoked by the force perturbations can be described by a linearized model. As deviations in our work are in line with those in existing studies (Dolan et al., 1993; Burdet et al., 2000; Darainy et al., 2007), we are able to derive a linearized model by first order Taylor series expansion of (1) about the unperturbed states $\boldsymbol{q}^*$, $\dot{\boldsymbol{q}}^*$, $\ddot{\boldsymbol{q}}^*$, $\boldsymbol{\tau}^*_{\text{int}}$, and $\boldsymbol{\tau}^*_{\text{ext}}$:

$$\Delta\boldsymbol{\tau}_{\text{int}} = \frac{\partial \boldsymbol{\tau}_{\text{int}}}{\partial \ddot{\boldsymbol{q}}} \Delta\ddot{\boldsymbol{q}} + \frac{\partial \boldsymbol{\tau}_{\text{int}}}{\partial \dot{\boldsymbol{q}}} \Delta\dot{\boldsymbol{q}} + \frac{\partial \boldsymbol{\tau}_{\text{int}}}{\partial \boldsymbol{q}} \Delta\boldsymbol{q} + \frac{\partial \boldsymbol{\tau}_{\text{int}}}{\partial \boldsymbol{\tau}_{\text{ext}}} \Delta\boldsymbol{\tau}_{\text{ext}} \ , \tag{8}$$

where all variational variables indicated by a Δ symbol represent the deviations from the unperturbed states, e.g., $\Delta\boldsymbol{q} = \boldsymbol{q}^* - \boldsymbol{q}$. Inserting (1) into (8) yields

$$\begin{aligned} \Delta\boldsymbol{\tau}_{\text{int}} = {} & M_q(\boldsymbol{q})\Delta\ddot{\boldsymbol{q}} + \frac{\partial C(\boldsymbol{q}, \dot{\boldsymbol{q}})}{\partial \dot{\boldsymbol{q}}} \Delta\dot{\boldsymbol{q}} \\ & + \left(\frac{\partial M_q(\boldsymbol{q})}{\partial \boldsymbol{q}} \ddot{\boldsymbol{q}} + \frac{\partial C(\boldsymbol{q}, \dot{\boldsymbol{q}})}{\partial \boldsymbol{q}} \right) \Delta\boldsymbol{q} - \Delta\boldsymbol{\tau}_{\text{ext}} \ . \end{aligned} \tag{9}$$

According to (2), the variational internal torques $\Delta\boldsymbol{\tau}_{\text{int}}$ depend on $\boldsymbol{\lambda}$, $\dot{\boldsymbol{\lambda}}$, and $\boldsymbol{a}$. Due to the limited duration of the estimation interval T_{est}, the variational muscle activations $\Delta\boldsymbol{a} = \boldsymbol{a}^* - \boldsymbol{a}$ can only consist of reflexive feedback muscle activations $\boldsymbol{a}_{\text{FB,r}}$. With $\Delta\boldsymbol{a} = \boldsymbol{f}(\boldsymbol{\lambda}, \dot{\boldsymbol{\lambda}})$ and $\boldsymbol{\lambda} = J_m(\boldsymbol{\lambda})\boldsymbol{q}$, first order Taylor series expansion of (5) yields

$$\Delta\boldsymbol{\tau}_{\text{int}} = -D_q(\boldsymbol{q}, \dot{\boldsymbol{q}}, \boldsymbol{a})\Delta\dot{\boldsymbol{q}} - K_q(\boldsymbol{q}, \dot{\boldsymbol{q}}, \boldsymbol{a})\Delta\boldsymbol{q} \tag{10}$$

with joint damping D_q and stiffness K_q defined as

$$D_q(\boldsymbol{q}, \dot{\boldsymbol{q}}, \boldsymbol{a}) = -\frac{\mathrm{d}\overline{\boldsymbol{\tau}}_{\text{FB}}}{\mathrm{d}\dot{\boldsymbol{q}}} \ , \quad K_q(\boldsymbol{q}, \dot{\boldsymbol{q}}, \boldsymbol{a}) = -\frac{\mathrm{d}\overline{\boldsymbol{\tau}}_{\text{FB}}}{\mathrm{d}\boldsymbol{q}} \ . \tag{11}$$

Due to inclusion of the reflexive feedback torques $\boldsymbol{\tau}_{\text{FB,r}}$, according to the terminology established in Latash and Zatsiorsky (1993), the matrices in (11) represent apparent impedance components. In this work, in order to highlight the exclusion of the voluntary feedback torques $\boldsymbol{\tau}_{\text{FB,v}}$, we refer to them as involuntary impedance components. For simplicity, we refer to the individual matrices D_q and K_q as joint damping and stiffness instead of involuntary joint damping and stiffness. Combining (9) and (10) yields

$$\begin{aligned}\Delta\boldsymbol{\tau}_{\text{ext}} = M_q(\boldsymbol{q})\Delta\ddot{\boldsymbol{q}} + \left(\frac{\partial C(\boldsymbol{q}, \dot{\boldsymbol{q}})}{\partial \dot{\boldsymbol{q}}} + D_q(\boldsymbol{q}, \dot{\boldsymbol{q}}, \boldsymbol{a})\right)\Delta\dot{\boldsymbol{q}} \\ + \left(\frac{\partial M_q(\boldsymbol{q})}{\partial \boldsymbol{q}}\ddot{\boldsymbol{q}} + \frac{\partial C(\boldsymbol{q}, \dot{\boldsymbol{q}})}{\partial \boldsymbol{q}} + K_q(\boldsymbol{q}, \dot{\boldsymbol{q}}, \boldsymbol{a})\right)\Delta\boldsymbol{q} \ .\end{aligned} \tag{12}$$

The elements of the partial derivative term that includes the inertia M_q are $\mathcal{O}(\ddot{q}\sin q)$ and the elements of the Coriolis and centrifugal forces C are $\mathcal{O}(\dot{q}^2)$ (Gomi and Kawato, 1997). Considering the limited duration of the estimation interval T_{est}, we assume that the contributions of the terms are negligible compared to those of the joint damping D_q and the joint stiffness K_q (Dolan et al., 1993). Inserting these assumptions into (12) yields

$$\Delta\boldsymbol{\tau}_{\text{ext}} = M_q(\boldsymbol{q})\Delta\ddot{\boldsymbol{q}} + D_q(\boldsymbol{q}, \dot{\boldsymbol{q}}, \boldsymbol{a})\Delta\dot{\boldsymbol{q}} + K_q(\boldsymbol{q}, \dot{\boldsymbol{q}}, \boldsymbol{a})\Delta\boldsymbol{q} \ . \tag{13}$$

In order to facilitate transfer to pHRI and applicability to our apparatus, we express (13) in Cartesian space:

$$\Delta\boldsymbol{u}_{\text{ext}} = M(\boldsymbol{x})\Delta\ddot{\boldsymbol{x}} + D(\boldsymbol{x}, \dot{\boldsymbol{x}}, \boldsymbol{a})\Delta\dot{\boldsymbol{x}} + K(\boldsymbol{x}, \dot{\boldsymbol{x}}, \boldsymbol{a})\Delta\boldsymbol{x} \tag{14}$$

$$\Delta\boldsymbol{u}_{\text{ext}} = J^{-\mathsf{T}}(\boldsymbol{q})\Delta\boldsymbol{\tau}_{\text{ext}} \ , \tag{15}$$

$$M(\boldsymbol{x}) = J^{-\mathsf{T}}(\boldsymbol{q})M_q(\boldsymbol{q})J^{-1}(\boldsymbol{q}) \ , \tag{16}$$

$$D(\boldsymbol{x}, \dot{\boldsymbol{x}}, \boldsymbol{a}) = J^{-\mathsf{T}}(\boldsymbol{q})D_q(\boldsymbol{q}, \dot{\boldsymbol{q}}, \boldsymbol{a})J^{-1}(\boldsymbol{q}) \ , \tag{17}$$

$$K(\boldsymbol{x}, \dot{\boldsymbol{x}}, \boldsymbol{a}) = J^{-\mathsf{T}}(\boldsymbol{q})K_q(\boldsymbol{q}, \dot{\boldsymbol{q}}, \boldsymbol{a})J^{-1}(\boldsymbol{q}) \ , \tag{18}$$

where $\boldsymbol{x}$ is the arm endpoint configuration, $\boldsymbol{u}_{\text{ext}}$ are the external endpoint forces, M, D, and K are the endpoint inertia, damping, and stiffness, and $J(\boldsymbol{q})$ is the Jacobian. As the endpoint inertia M describes the relationship between an external force acting on the arm endpoint and the resulting acceleration, it is an apparent inertia. For simplicity, in this work, we refer to it as inertia.

The considered problem consists of the estimation of the involuntary impedance components M, D, and K in a limited estimation interval $[0, T_{\text{est}}]$. This is to be achieved given the perturbed observations $\{\boldsymbol{x}, \dot{\boldsymbol{x}}, \ddot{\boldsymbol{x}}, \boldsymbol{u}_{\text{ext}}\}$, which are evoked by force perturbations, and requires the estimation of the variational dynamics $\Delta\boldsymbol{x}$, $\Delta\dot{\boldsymbol{x}}$, $\Delta\ddot{\boldsymbol{x}}$, and $\Delta\boldsymbol{u}_{\text{ext}}$.

3. INVOLUNTARY IMPEDANCE ESTIMATION

This section presents the successive steps necessary for the estimation of the involuntary impedance components.

3.1 Variational dynamics

According to the minimum jerk principle (Flash and Hogan, 1985), the CNS optimizes the endpoint trajectory of the arm in a point to point movement by minimization of the total endpoint jerk. In this work, we capitalize on the effects of the minimum jerk principle by designing the perturbation jerk in such a way that the jerk frequency content of the evoked feedback behavior lies outside the jerk frequency content of the unperturbed movements. Thus, we are able to estimate the feedback behavior in the form of the variational jerk $\Delta\dddot{\boldsymbol{x}}$ by applying an appropriately configured high pass filter to the jerk of the perturbed movements. In order to achieve maximum flatness of the pass band, i.e., minimum attenuation of the variational jerk $\Delta\dddot{\boldsymbol{x}}$, we use a Butterworth high pass filter. The cut-off frequency $f_{\text{c,HP}}$ is defined in accordance with the frequency content of the jerk of the unperturbed and perturbed movements. The filter is applied bi-directionally to guarantee zero phase distortion. The high pass filtered jerk $\dddot{\boldsymbol{x}}_{\text{HP}}$ provides the estimated variational jerk $\Delta\dddot{\hat{\boldsymbol{x}}}$ and the estimated variational kinematics $\Delta\ddot{\hat{\boldsymbol{x}}}$, $\Delta\dot{\hat{\boldsymbol{x}}}$, and $\Delta\hat{\boldsymbol{x}}$ are obtained by integration. Due to the limited duration of the estimation interval T_{est}, high estimation accuracy is achieved despite integration drift effects.

As the apparatus in our experiments is controlled by an admittance control scheme, the estimated variational external forces $\Delta\hat{\boldsymbol{u}}_{\text{ext}}$ can be calculated with

$$\boldsymbol{u}_{\text{ext}} = \boldsymbol{u}_{\text{pert}} - (\boldsymbol{u}_{\text{adm}} + M_{\text{handle}}\ddot{\boldsymbol{x}}) \ , \tag{19}$$

$$\boldsymbol{u}_{\text{adm}} = M_{\text{adm}}\ddot{\boldsymbol{x}} + D_{\text{adm}}\dot{\boldsymbol{x}} \ , \tag{20}$$

where $\boldsymbol{u}_{\text{pert}}$ is the perturbation force and $\boldsymbol{u}_{\text{adm}}$ is the force applied to the admittance. The matrix M_{handle} is the handle inertia, and the matrices M_{adm} and D_{adm} are the admittance inertia and damping. Inserting (20) into (19) yields the estimated variational external forces

$$\Delta\hat{\boldsymbol{u}}_{\text{ext}} = \boldsymbol{u}_{\text{pert}} - (M_{\text{adm}} + M_{\text{handle}})\Delta\ddot{\hat{\boldsymbol{x}}} - D_{\text{adm}}\Delta\dot{\hat{\boldsymbol{x}}} \ , \tag{21}$$

which complete the necessary variational dynamics for the estimation of the involuntary impedance components.

3.2 Perturbation design

The perturbation jerk must be designed in such a way that it meets two essential requirements. Its frequency content must lie outside the frequency content of the jerk of the unperturbed movements and it must be smooth enough to guarantee minimal distortion due to kinesthetic rendering and data processing. In order to fulfill these requirements, we divide the duration of the perturbation T_{pert} into three equally long sections, each of duration $T_{\text{p}} = T_{\text{pert}}/3$ and design the normalized perturbation jerk $\dot{u}_{\text{p}}$ through concatenation of multiple sinusoidal functions:

$$\dot{u}_{\text{p}} = \begin{cases} \dfrac{1}{2}\sin\left(\left(\dfrac{t_{\text{p,1}}}{T_{\text{p}}} + \dfrac{3}{2}\right)\pi\right) + \dfrac{1}{2} & \forall\ t_{\text{p,1}} \in [0, T_{\text{p}}] \\ \sin\left((\dfrac{t_{\text{p,2}}}{T_{\text{p}}} + \dfrac{1}{2})\pi\right) & \forall\ t_{\text{p,2}} \in\ ]0, T_{\text{p}}] \\ \dfrac{1}{2}\sin\left(\left(\dfrac{t_{\text{p,3}}}{T_{\text{p}}} + \dfrac{3}{2}\right)\pi\right) - \dfrac{1}{2} & \forall\ t_{\text{p,3}} \in\ ]0, T_{\text{p}}] \end{cases} , \tag{22}$$

in which $t_{\text{p,1}} = t - t_0$, $t_{\text{p,2}} = t_{\text{p,1}} - T_{\text{p}}$, and $t_{\text{p,3}} = t_{\text{p,2}} - T_{\text{p}}$. Fig. 1 presents the normalized perturbation jerk $\dot{u}_{\text{p}}$ and

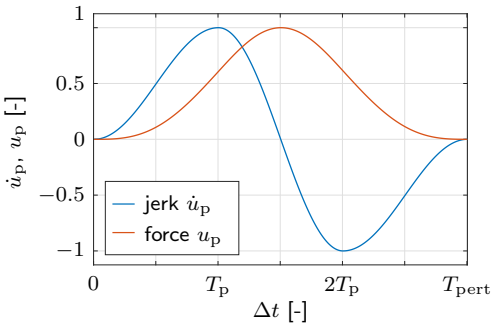

Fig. 1. Normalized perturbation jerk $\dot{u}_\mathrm{p}$ and force u_p.

the integrated normalized perturbation force u_p, which is scaled in order to obtain the perturbation force

$$\boldsymbol{u}_\mathrm{pert} = A_\mathrm{pert} u_\mathrm{p} [\cos\phi_\mathrm{pert}, \sin\phi_\mathrm{pert}]^\mathsf{T} \,, \tag{23}$$

where A_pert and ϕ_pert are the amplitude and angle.

3.3 Involuntary impedance components

The involuntary impedance components M, D, and K depend on $\boldsymbol{x}$, $\dot{\boldsymbol{x}}$, and $\boldsymbol{a}$. In this work, due to the limited duration of the estimation interval T_est, we assume that they are constant for $\Delta t \in [0, T_\mathrm{est}]$ and approximate them by the involuntary impedance parameters $\overline{M}$, $\overline{D}$, and $\overline{K}$. This approach is common to impedance estimation studies and similarly applied to significantly longer estimation intervals than the one in this work (Gomi and Kawato, 1997; Lakatos et al., 2011; Erden and Billard, 2015). Concatenation of the elements of $\overline{M}$, $\overline{D}$, and $\overline{K}$ in the vector of unknown parameters

$$\begin{aligned}\boldsymbol{\zeta} = \big[&\overline{M}_{11}, \overline{M}_{12}, \overline{M}_{21}, \overline{M}_{22}, \overline{D}_{11}, \overline{D}_{12}, \\ &\overline{D}_{21}, \overline{D}_{22}, \overline{K}_{11}, \overline{K}_{12}, \overline{K}_{21}, \overline{K}_{22}\big]^\mathsf{T}\end{aligned} \tag{24}$$

allows expression of (14) by the identification model

$$A\boldsymbol{\zeta} = \boldsymbol{b} \,, \tag{25}$$

where A is the observation matrix and $\boldsymbol{b}$ is the output vector. For an estimation interval of N samples

$$A = \big[X^\mathsf{T}(1), X^\mathsf{T}(2), \ \dots \ , X^\mathsf{T}(N)\big]^\mathsf{T} \,, \tag{26}$$

$$\boldsymbol{b} = \Big[\Delta\hat{\boldsymbol{u}}^\mathsf{T}_\mathrm{ext}(1), \Delta\hat{\boldsymbol{u}}^\mathsf{T}_\mathrm{ext}(2), \ \dots \ , \Delta\hat{\boldsymbol{u}}^\mathsf{T}_\mathrm{ext}(N)\Big]^\mathsf{T} \,, \tag{27}$$

and the matrix of independent variables

$$X = \frac{\partial(\overline{M}\Delta\ddot{\hat{\boldsymbol{x}}} + \overline{D}\Delta\dot{\hat{\boldsymbol{x}}} + \overline{K}\Delta\hat{\boldsymbol{x}})}{\partial\boldsymbol{\zeta}} \,. \tag{28}$$

Considering (25) - (28), the estimated vector of unknown parameters $\hat{\boldsymbol{\zeta}}$ is given by the least squares solution

$$\hat{\boldsymbol{\zeta}} = (A^\mathsf{T}A)^{-1}A^\mathsf{T}\boldsymbol{b} \,. \tag{29}$$

Due to the limited duration of the estimation interval T_est, which implies a limited duration of the perturbation T_pert, the perturbation does not possess sufficient richness of frequency components to guarantee persistent excitation (Söderström and Stoica, 1989). A common approach for the compensation of the consequences of a non-persistent excitation is the a priori estimation of the body segment parameters (BSPs) (Gomi and Kawato, 1997; Darainy et al., 2007; Lakatos et al., 2011), which only marginally influences the accuracy of the estimation of the impedance parameters (Gomi and Osu, 1998). A comparison of nine different methods for the estimation of BSPs is presented in Piovesan et al. (2013). As such a comparison exceeds the scope of this work, we use realistic anthropometric data (Franklin et al., 2007) and inverse dynamics to a priori calculate the estimated inertia $\hat{M}_\mathrm{BSP}$.

The intrinsic feedback behavior of the endpoint of the arm possesses spring-like characteristics due to the elastic properties of the individual muscles. Thus, the intrinsic feedback forces possess zero curl and the intrinsic stiffness is symmetric (Shadmehr and Arbib, 1992). The reflexive feedback forces may possess non-zero curl components, which can only be caused by heteronymous inter-muscular reflex arcs (Hogan, 1985). As the resulting antisymmetric stiffness components are significantly smaller than the symmetric components, the reflexive feedback behavior still possesses predominantly spring-like characteristics (Mussa-Ivaldi et al., 1985). As the estimation intervals in these studies are significantly longer than the one in this work, we assume that the stiffness $\overline{K}$ for $\Delta t \in [0, T_\mathrm{est}]$ is symmetric. With the estimated inertia $\hat{M}_\mathrm{BSP}$, the vector of the unknown parameters $\boldsymbol{\zeta}$ reduces to

$$\overline{\boldsymbol{\zeta}} = \big[\overline{D}_{11}, \overline{D}_{12}, \overline{D}_{21}, \overline{D}_{22}, \overline{K}_{11}, \overline{K}_{12}, \overline{K}_{22}\big]^\mathsf{T} \,, \tag{30}$$

the matrix of independent variables X reduces to

$$\overline{X} = \frac{\partial(\overline{D}\Delta\dot{\hat{\boldsymbol{x}}} + \overline{K}\Delta\hat{\boldsymbol{x}})}{\partial\overline{\boldsymbol{\zeta}}} \,, \tag{31}$$

and the elements of the output vector b_i are

$$\overline{b}_i = \Delta\hat{\boldsymbol{u}}_\mathrm{ext} - \hat{M}_\mathrm{BSP}\Delta\ddot{\hat{\boldsymbol{x}}}, \quad i = 1, 2, \ \dots \ , N \,. \tag{32}$$

Inclusion in (29) provides the estimated damping $\hat{\overline{D}}$ and stiffness $\hat{\overline{K}}$, which, in combination with the inertia $\hat{M}_\mathrm{BSP}$, constitute the involuntary impedance parameters.

4. SIMULATION

We validate the isolation of the feedback behavior with a simulated, neuromechanical model of the human arm (Franklin et al., 2007). We use this model in order to enable comparability with existing studies, in which its plausibility has been demonstrated (Franklin et al., 2008). It simulates two-dimensional, transversal movement of a two-link, six-muscle arm through calculation of muscle activities and resulting muscle tensions. By simulating each movement twice, once as an unperturbed and once as a perturbed movement, we are able to use it to validate the estimation of the variational dynamics.

4.1 Human arm model

The dynamics of the model are given by (1) and (2) and the muscle tensions $\boldsymbol{m}$ are composed of two terms:

$$\boldsymbol{m} = \boldsymbol{m}_\mathrm{A} + \boldsymbol{m}_\mathrm{IMP} \,, \tag{33}$$

where $\boldsymbol{m}_\mathrm{A}$ and $\boldsymbol{m}_\mathrm{IMP}$ represent the muscle tensions due to the muscle activations $\boldsymbol{a}$ and the mechanical impedance. The former are assumed to be identical to the motor commands, i.e., the muscle activations $\boldsymbol{a}$, as defined in (3). The muscle tensions due to the mechanical impedance

$$\boldsymbol{m}_\mathrm{IMP} = D_m\dot{\boldsymbol{e}}_m + K_m\boldsymbol{e}_m \tag{34}$$

with

$$D_m = K_m/12 \,, \quad K_m = K_0 + K_1\boldsymbol{a} \,, \tag{35}$$

where D_m, K_m, and $\boldsymbol{e}_m$ represent damping, stiffness, and tracking errors with respect to the desired trajectory $\boldsymbol{q}_\mathrm{d}$

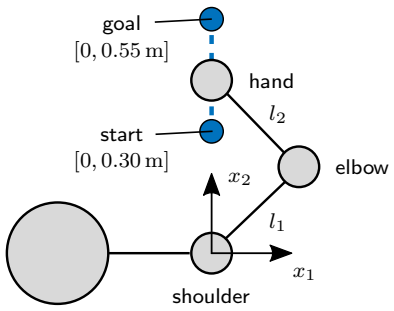

Fig. 2. Schematic of simulated point to point movements.

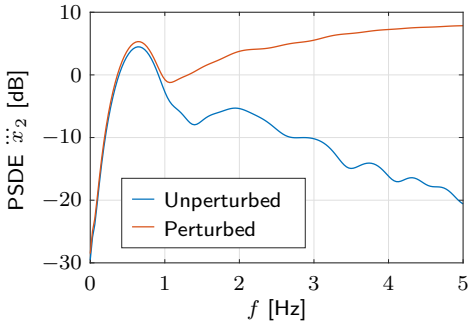

Fig. 3. PSDEs of the principal movement axis jerk $\dddot{x}_2$.

at muscle level and the matrices K_0 and K_1 contain constant intrinsic stiffness parameters. The feedforward muscle activations $\boldsymbol{a}_{\mathrm{FF}}$ are calculated with the inverse kinematics and dynamics of a positional data set of 50 two-dimensional point to point arm movements, provided by the authors of Franklin et al. (2007). The hand is moved along the sagittal axis from $\boldsymbol{x}_{\mathrm{start}} = [0, 0.30]^{\mathsf{T}}\,\mathrm{m}$ to $\boldsymbol{x}_{\mathrm{goal}} = [0, 0.55]^{\mathsf{T}}\,\mathrm{m}$, as illustrated in Fig. 2. The feedback muscle activations $\boldsymbol{a}_{\mathrm{FB}}$ are modeled by Proportional-Derivative (PD) control that depends on the tracking errors $\boldsymbol{e}_m$, the respective derivatives $\dot{\boldsymbol{e}}_m$ and a constant feedback delay $\delta_{\mathrm{s}} = 60$ ms. The signal-dependent noise $\boldsymbol{a}_{\mathrm{N}}$ is modeled by zero mean Brownian motion.

4.2 Simulation design

For conformity with the behavior observed during our experiment, we set the duration of the movements to 3 s and resample the provided positional data set accordingly. The simulated manipulandum inertia and damping are set according to the admittance inertia $M_{\mathrm{adm}} = \mathrm{diag}\{5, 5\}$ kg and damping $D_{\mathrm{adm}} = \mathrm{diag}\{15, 15\}$ Ns/m of our apparatus. The duration of the perturbation T_{pert} is set to 150 ms. The perturbation is initiated as soon as the hand reaches $x_2 = 0.4$ m, which equals a distance of 0.1 m along the axis of the principal movement (see Fig. 2). The perturbation amplitude A_{pert} is set to 15 N. Due to the admittance inertia M_{adm} and damping D_{adm}, the limited duration of the estimation interval T_{est}, and the perturbation design, this evokes maximum deviations within the estimation interval $[0, T_{\mathrm{est}}]$ (reported in mean (std dev): 6.1 (1.8) mm along x_1-axis, 5.9 (1.7) mm along x_2-axis) that are in line with those applied in existing studies (Dolan et al., 1993; Burdet et al., 2000; Darainy et al., 2007). In order to avoid small deviations due to perturbations parallel to the axes of the coordinate system, the perturbation angles ϕ_{pert} are defined as $\Phi_{\mathrm{pert}} = \{30, 60, 120, 150, 210, 240, 300, 330\}$ deg. Each angle ϕ_{pert} is executed 10 times, which results in a total of 80 individual trials, of which each is composed of an unperturbed and a perturbed version of the movement. For conformity with the experiment, the simulated signals are filtered using a fifth order Savitzky-Golay filter with a cut-off frequency of $f_{\mathrm{c,SG}} = 30$ Hz.

4.3 Validation of variational dynamics

In order to determine the cut-off frequency $f_{\mathrm{c,HP}}$ of the Butterworth high pass filter, we apply Welch's method to calculate the power spectral density estimates (PSDEs) of the jerk $\dddot{\boldsymbol{x}}$ of the unperturbed and perturbed movements. We use this approximation technique in order to allow for analogous application to the data of the experiment. As the unperturbed movements along the lateral axis are negligible compared to those along the sagittal axis, i.e., the axis of the principal movement, we focus on the respective jerk $\dddot{x}_2$. The mean PSDE results are presented in Fig. 3. The unperturbed PSDE reaches its spectral peak at 0.6385 Hz and then decreases rapidly. The perturbed PSDE possesses almost identical values below a frequency of approximately 1 Hz. Above this frequency, the PSDEs diverge and its values are significantly larger than those of the unperturbed PSDE. Thus, the frequency content of the jerk of the evoked feedback behavior lies almost completely above 1 Hz. Furthermore, as the unperturbed PSDE has already passed its spectral peak and decreased to -2.913 dB at this frequency, the contributions of the jerk of the unperturbed movement above this frequency are marginal. Therefore, we set the cut-off frequency $f_{\mathrm{c,HP}}$ of the high pass filter to 1 Hz and apply it to the jerk of the perturbed movement to obtain the estimated variational jerk $\Delta\hat{\dddot{\boldsymbol{x}}}$. In order to achieve maximum attenuation for the stop band of the high pass filter, we set the order of the high pass filter to the highest possible value $n_{\mathrm{HP}} = 5$.

The accuracy of the estimated variational dynamics $\Delta\hat{\boldsymbol{x}}$, $\Delta\hat{\dot{\boldsymbol{x}}}$, $\Delta\hat{\ddot{\boldsymbol{x}}}$, and $\Delta\hat{\boldsymbol{u}}_{\mathrm{ext}}$ is assessed with the normalized root mean square errors (NRMSEs), which are calculated with the difference of the estimated and the simulated values. The difference is normalized with the largest value of the respective variable in the estimation interval of interest, which is defined by $\Delta t \in [0, 150\ \mathrm{ms}]$ for this validation. The results in Fig. 4 show that the NRMSEs all increase for increasing Δt. Nonetheless, the maximum values of the estimated variational kinematics $\Delta\hat{\boldsymbol{x}}$, $\Delta\hat{\dot{\boldsymbol{x}}}$, and $\Delta\hat{\ddot{\boldsymbol{x}}}$ are below 7.5% (and in case of $\Delta\hat{\boldsymbol{x}}$ and $\Delta\hat{\ddot{\boldsymbol{x}}}$ even below 5%). The results in Fig. 4 also show that the NRMSE of the estimated variational external forces $\Delta\hat{\boldsymbol{u}}_{\mathrm{ext}}$ increases approximately twice as fast as all the other NRMSEs. This is plausible, as its calculation in (19) is based on the estimated variational accelerations $\Delta\hat{\ddot{\boldsymbol{x}}}$ and velocities $\Delta\hat{\dot{\boldsymbol{x}}}$. Nonetheless, its maximum value at the end of the interval is still below 15%. For the perturbed movements of the simulated arm model, a 5% NRMSE in $\Delta\hat{\boldsymbol{x}}$ approximately corresponds to an error of 0.3 mm and a 15% NRMSE in $\Delta\hat{\boldsymbol{u}}_{\mathrm{ext}}$ approximately corresponds to an error of 0.4 N.

In the implementation of the simulated, neuromechanical model of the human arm, there is no clear distinction between reflexive and voluntary feedback. Instead, both are combined in the feedback muscle activations $\boldsymbol{a}_{\mathrm{FB}}$, which possess a delay of $\delta_{\mathrm{s}} = 60$ ms. As this delay is much

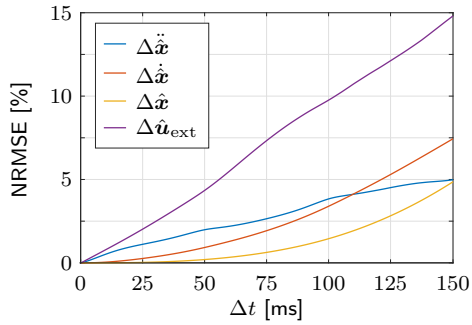

Fig. 4. NRMSEs of the estimated variational dynamics.

smaller than the duration of our estimation interval T_{est}, we cannot validate the estimated involuntary impedance parameters $\overline{\hat{M}}$, $\overline{\hat{D}}$, and $\overline{\hat{K}}$ with the simulated intrinsic impedance components. Thus, we instead evaluate the performance of this estimation with experimental data.

5. EXPERIMENT

In order to evaluate the applicability to experimental data, we conduct an experiment with five human participants. The estimation of the variational dynamics $\Delta\boldsymbol{x}$, $\Delta\dot{\boldsymbol{x}}$, $\Delta\ddot{\boldsymbol{x}}$, and $\Delta\boldsymbol{u}_{\text{ext}}$ is performed analogously to the validation with simulated data. In this section, we focus on the estimation of the involuntary impedance parameters $\overline{D}$ and $\overline{K}$.

5.1 Apparatus & data processing

The apparatus consists of two linear, orthogonally aligned single rail stages (*Copley Controls Thrusttube Module*) that span a 2-DoF workspace of ± 0.15 m and each provide position data with a precision of 1 μm. On top of the cart of the upper module, a vertical handle with a 6-DoF force-torque sensor (*JR3-67M25*) is mounted to measure horizontal forces. Visual feedback is implemented with the Psychophysics Toolbox (Brainard, 1997) and shown on a computer screen mounted behind the apparatus.

Haptic interaction is enabled by the admittance control scheme defined in (20), where $M_a = \text{diag}\{5, 5\}$ kg and $D_a = \text{diag}\{15, 15\}$ Ns/m. Precise rendering of the position is ensured by a high gain PD controller, implemented in *Matlab/Simulink* and executed on a *Linux* system with a *RT-preempt* real-time kernel. The sample rate is $f_s = 4$ kHz and inputs to the Thrusttube Modules are downsampled to 2 kHz to adhere to hardware limitations. The signals are filtered using a fifth order Savitzky-Golay filter with a cut-off frequency of $f_{\text{c,SG}} = 30$ Hz.

5.2 Participants & experiment design

A total of five male participants volunteered to take part in this experiment. All participants were right handed and had normal or corrected-to-normal vision. The age of the participants in mean (std dev) was 28.20 (1.79) years at the time of the experiment. Informed written consent was obtained from all participants before they took part in the experiment. The research ethics were obtained from the ethics committee at the Technical University of Munich.

The participants were seated in front of the apparatus and instructed to grasp the handle with their right hand.

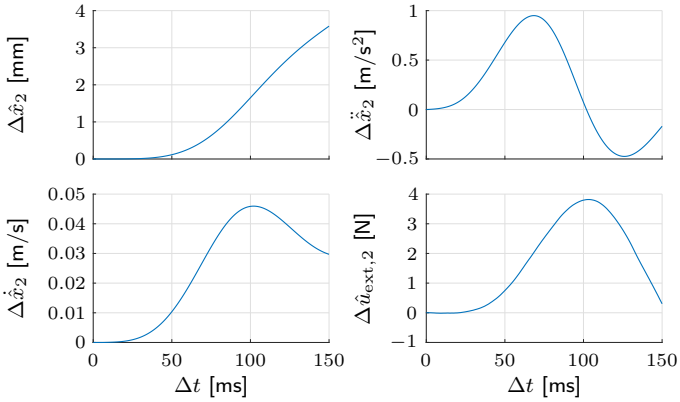

Fig. 5. Exemplary set of estimated variational dynamics.

Their arm was supported against gravity and restrained to movements in the horizontal plane by a sling attached to the ceiling. The goal of the point to point movement was displayed on the screen behind the apparatus and the current cart position was illustrated by a green dot. The participants were instructed to complete 100 point to point movements at their own pace. Each perturbation angle ϕ_{pert} was executed three times. The order of the perturbation angles was randomized and the 24 perturbed trials were distributed randomly. The participants were informed of the general existence of the perturbations and were instructed to not react to them preemptively.

5.3 Evaluation of involuntary impedance parameters

Due to the design of the perturbation, specifically the slow rise in acceleration, the onset of the perturbation is followed by an interval of duration T_{dev} that does not possess noticeable deviations. This effect can be observed in the exemplary set of estimated variational dynamics in Fig. 5. For an interval of duration $T_{\text{dev}} = 35$ ms, the mean (std dev) deviations are 0.028 (0.012) mm along the x_1-axis and 0.030 (0.010) mm along the x_2-axis. As these values are negligibly small, in this work, the delay of the voluntary feedback muscle activations $\boldsymbol{a}_{\text{FB,v}}$ is assumed $\delta_{\text{v,dev}} = \delta_{\text{v}} + T_{\text{dev}} = 115$ ms $+ 35$ ms $= 150$ ms and the duration of the estimation interval $T_{\text{est}} = \delta_{\text{v,dev}} = 150$ ms.

Table 1 contains the mean (std dev) results of the elements of the estimated damping $\overline{\hat{D}}$ and the estimated stiffness $\overline{\hat{K}}$. As the estimated inertia $\hat{M}_{\text{BSP}}$ is calculated a priori based on inverse kinematics and realistic anthropometric data from the literature (Franklin et al., 2007), it is not listed. In both of the estimated matrices, the diagonal elements are positive and the non-diagonal elements are negative. This is a result of the transformation from joint space to Cartesian space via the Jacobian $J(\boldsymbol{q})$. In the estimated stiffness matrix $\overline{\hat{K}}$, the stiffness element $\overline{\hat{K}}_{22}$ is significantly larger than all of the remaining elements. This is a result of the definition in (18), which contains both the endpoint muscle stiffness as well as a geometric stiffness term that

Table 1. Estimation results in mean (std dev).

Damping $\overline{\hat{D}}$ [Ns/m]		**Stiffness $\overline{\hat{K}}$ [N/m]**	
10.98 (4.85)	-7.94 (3.26)	110.52 (48.54)	-106.05 (62.91)
-8.54 (4.16)	6.75 (4.27)	-106.04 (62.91)	313.75 (77.46)

is defined by the internal torques. As the latter are much larger along the axis of the principal movement, the same applies to the respective estimated stiffness element.

The results in Table 1 are of the same order of magnitude as those reported in similar studies (Tsuji et al., 1995; Tanaka et al., 2003; Erden and Billard, 2015). In all three of these studies, the estimated damping results are approximately twice as large as the results in Table 1. This difference could be caused by the reduced duration of the estimation interval T_{est} or the damping D_{adm} supplied by the admittance control scheme. In Tsuji et al. (1995) and Tanaka et al. (2003), the estimated stiffness results are similar to those obtained for the stiffness element $\overline{\hat{K}}_{11}$. In Erden and Billard (2015), they are significantly larger. This difference is plausible, as the execution of the manual welding task requires much higher accuracy. In summary, the comparison with similar studies indicates plausibility of the results in Table 1 for multi-joint arm movements.

6. CONCLUSION

In this work, we present a method for the estimation of involuntary impedance during multi-joint arm movements. We apply external force perturbations to evoke deviations during point to point arm movements. The perturbations are specifically designed to evoke feedback behavior that can be isolated by application of a high pass Butterworth filter to the jerk of the perturbed movements. The duration of the estimation interval is limited to guarantee exclusion of voluntary feedback. The impedance components within the estimation interval are approximated by impedance parameters and estimated through least squares analysis. The analysis of the NRMSEs of the estimated variational dynamics within the validation with simulated data shows the accuracy of the isolation of the feedback behavior. Experimental data of an experiment with five human participants is used to evaluate the estimation of the involuntary impedance parameters and demonstrate the applicability of the method to real data. In future work, we will apply the proposed method for the estimation and analysis of involuntary impedance modulation strategies.

REFERENCES

Brainard, D.H. (1997). The psychophysics toolbox. *Spatial vision*, 10, 433–436.

Burdet, E., Osu, R., Franklin, D., Yoshioka, T., Milner, T., and Kawato, M. (2000). A method for measuring endpoint stiffness during multi-joint arm movements. *Journal of biomechanics*, 33(12), 1705–1709.

Darainy, M., Towhidkhah, F., and Ostry, D.J. (2007). Control of hand impedance under static conditions and during reaching movement. *Journal of neurophysiology*, 97(4), 2676–2685.

Dolan, J.M., Friedman, M.B., and Nagurka, M.L. (1993). Dynamic and loaded impedance components in the maintenance of human arm posture. *IEEE transactions on systems, man, and cybernetics*, 23(3), 698–709.

Erden, M.S. and Billard, A. (2015). Hand impedance measurements during interactive manual welding with a robot. *IEEE transactions on robotics*, 31(1), 168–179.

Flash, T. and Hogan, N. (1985). The coordination of arm movements: an experimentally confirmed mathematical model. *Journal of neuroscience*, 5(7), 1688–1703.

Franklin, D.W., Burdet, E., Tee, K.P., Osu, R., Chew, C.M., Milner, T.E., and Kawato, M. (2007). Supplementary material for cns learns stable, accurate and efficient movements using a simple algorithm.

Franklin, D.W., Burdet, E., Tee, K.P., Osu, R., Chew, C.M., Milner, T.E., and Kawato, M. (2008). Cns learns stable, accurate, and efficient movements using a simple algorithm. *Journal of neuroscience*, 28(44).

Franklin, D.W. and Wolpert, D.M. (2011). Computational mechanisms of sensorimotor control. *Neuron*, 72(3), 425–442.

Gomi, H. and Kawato, M. (1997). Human arm stiffness and equilibrium-point trajectory during multi-joint movement. *Biological cybernetics*, 76(3), 163–171.

Gomi, H. and Osu, R. (1998). Task-dependent viscoelasticity of human multijoint arm and its spatial characteristics for interaction with environments. *Journal of neuroscience*, 18(21), 8965–8978.

Hogan, N. (1985). The mechanics of multi-joint posture and movement control. *Biological cybernetics*, 52(5), 315–331.

Lakatos, D., Petit, F., and Van Der Smagt, P. (2011). Conditioning vs. excitation time for estimating impedance parameters of the human arm. In *2011 IEEE-RAS International Conference on Humanoid Robots*, 636–642.

Latash, M.L. and Zatsiorsky, V.M. (1993). Joint stiffness: Myth or reality? *Human movement science*, 12(6), 653–692.

Matthews, P.B. (1991). The human stretch reflex and the motor cortex. *Trends in neurosciences*, 14(3), 87–91.

Merton, P. and Morton, H. (1980). Stimulation of the cerebral cortex in the intact human subject. *Nature*, 285(5762), 227.

Mussa-Ivaldi, F.A., Hogan, N., and Bizzi, E. (1985). Neural, mechanical, and geometric factors subserving arm posture in humans. *Journal of neuroscience*, 5(10), 2732–2743.

Piovesan, D., Pierobon, A., DiZio, P., and Lackner, J.R. (2013). Experimental measure of arm stiffness during single reaching movements with a time-frequency analysis. *Journal of neurophysiology*, 110(10), 2484–2496.

Shadmehr, R. and Arbib, M.A. (1992). A mathematical analysis of the force-stiffness characteristics of muscles in control of a single joint system. *Biological cybernetics*, 66(6), 463–477.

Slifkin, A.B. and Newell, K.M. (1999). Noise, information transmission, and force variability. *Journal of experimental psychology*, 25(3), 837.

Söderström, T. and Stoica, P. (1989). System identification.

Tanaka, Y., Tsuji, T., and Kaneko, M. (2003). Task readiness impedance in human arm movements for virtual ball-catching task. In *2003 Annual Conference of the IEEE Industrial Electronics Society*, volume 1, 478–483.

Tee, K.P., Burdet, E., Chew, C.M., and Milner, T.E. (2004). A model of force and impedance in human arm movements. *Biological cybernetics*, 90(5), 368–375.

Todorov, E. and Jordan, M.I. (2002). Optimal feedback control as a theory of motor coordination. *Nature neuroscience*, 5(11), 1226.

Tsuji, T., Morasso, P.G., Goto, K., and Ito, K. (1995). Human hand impedance characteristics during maintained posture. *Biological cybernetics*, 72(6), 475–485.